Proceedings World Geothermal Congress 2015
Melbourne, Australia, 19-25 April 2015

Multi-scalar Analysis of the Porous Network for Deep Geothermal Reservoir: Petrophysical Properties of Fault Zones

Yves Géraud, Lionel Bertrand, Sébastien Haffen, Bastien Walter, Edouard Le Garzic, Joachim Place, Michel Rosener, Marc Diraison, Fabrice Surma

École Nationale Supérieure de Géologie de Nancy, France

yves.géraud@univ-lorraine.fr, lionel.bertrand@univ-lorraine.fr, sébastien.haffen@univ-lorraine.fr, bastien.walter@univ-lorraine.fr,

Keywords: basement, granite, fault zone, porosity, permeability, thermal conductivity

ABSTRACT

In EGS reservoirs, fault zones are considered being the structures controlling deep flow at the reservoir scale in low porosity materials such as granite or metamorphic rocks. Using a large set of petrophysical properties (porosity, density, permeability, thermal conductivity, heat capacity, Vp, Vs) measured on cores and on other outcrop samples, a model fault zone with induced petrophysical properties is proposed. The different parts composing the fault zone are the following: the fault core or gauge zone, the damage zone, and the protolith. These parts are usually heterogeneous and show different physical properties. The damage zone is a potential high permeability channel and could become the main pathway for fluids if secondary minerals seal the fault core. Porosity is the lowest within the protolith with a value between 0.5 and one percent. However, the porosity value can be as high as 15 percent in the fault zone. Permeability values range from 10^{-20} m^2 in fresh granite to 10^{-14} m^2 in the fault core. In addition, the thermal conductivity values range from 1.5 $WK^{-1}m^{-1}$ to 3.7 $WK^{-1}m^{-1}$. Finally, variations in specific surface are set to over two orders of magnitude. Since the lowest values of petrophysical parameters usually characterize the fresh granite far from fault zones, physical properties could show how the variations spread over their whole respective ranges within these fault zones. All of these results could be used to define the role of each part in hydro-mechanical or chemical fluid rock interactions and the behavior of fault zone during fluid flow. Models of the porosity development and of fluid and heat fluxes are also proposed.

1. INTRODUCTION

To produce electricity from geothermal resource, the fluid temperature must be higher than 170°C. For sedimentary basins, the basement could be the main target to explore. There are two kinds of reservoirs: the fault and fractures networks under extensive reactivation and the weathered level developed at the interface between the basement and its sedimentary cover (Younes, 1998). The heat exchange between the rock and the exploitation fluid occurs at the boundaries of the porosity network. In both types of reservoirs, porosity and fluid transfer properties are mainly described as dependent on the fracture network properties. However, the matrix porosity could have an important contribution especially for the high porosity (higher than 10 percent) part of the network. Furthermore, the matrix porosity could likewise influence the long term behaviour.

In this paper, the main objectives were to propose a description of the different parts of the matrix porosity network and to propose a model for the porosity development and for the inferred petrophysical properties such as permeability, thermal conductivity or Vp/Vs. The basement interface of the Soultz-sous-Forêts geothermal field was cored from 1200 metres deep to 2200 metres deep of the Rhine Graben (Alsace France) (Genter and Traineau, 1992). From a set of 100 samples, the petrophysical properties were determined and presented in this study. The petrophysical properties were measured for different strain and alteration facies and their relationship for a model of behaviour was proposed.

2. STRUCTURAL NETWORK DEVELOPED WITHIN THE SOULTZ-SOUS-FORÊTS GRANITE.

The deep geothermal experimental site of Soultz-sous-forêts is located in the North of the French part of the Upper Rhine Graben (Alsace, France). It is composed of a set of three operational deep boreholes (GPK2, GPK3 and GPK4), reaching the depth of 5000 metres, and a set of three recognition boreholes (GPK1, EPS1 and 4550). Only EPS1 was completely cored down to 2450 metres depth.

The fracture network was extensively analysed and three clusters of faults and fractures were recognized in the basement from analysis of the different sets of diagraphic data. The three clusters were located in the following areas: the interface with the sedimentary infilling, 3000 metres depth, and the bottom of the borehole at 500 metres depth (Figure 1). Four main petrographic facies were recognized from top to the bottom: a standard porphyritic granite, a standard granite with intense vein alteration, biotite and amphibole rich granite becoming a standard granite, and a two mica granite (Figure 1). Only EPS1 was cored along its length. The basement was intersected between 1400 and 2400 metres depth and samples were obtained for the upper part of the batholith in the zone of weathering processes development and for the upper part of fracture network. Both parts contributed to the first cluster determined from the diagraphic data and form the shallowest reservoir within the batholith (Dezayes et al., 2010). In this first cluster, weathering processes were associated to a fracture set with a low dipping in the upper part of the batholith and were marked by the hematite mineral with the highest development in the first 250 metres of the batholith (Figure 2). Assuming that the hematite mineral was a mark of the weathering effect, the hematite mineral could affect 500 metres of granite below the sedimentary cover-basement interfaces (Just and Kontny, 2012). Below 1700 metres depth, a set of high dipping structures were picked on cores and on diagraphic images. The development of secondary alteration phases, mainly induced by hydrothermal alteration, were observed (Ledesert et al., 2010 and Bartier et al., 2008). A summary of the petrographic facies can be found on Table 1, with the description of the main magmatic facies and a set of five facies used to describe the material intersected by the borehole.

Quartz and illite have fairly similar distributions. Illite is mainly present at the fault zone at 1650 m to 1700 m. It is described along certain fractures of the upper part of batholith and for different levels of fractures in the lower part of the borehole. Quartz has three preferential precipitation zones: near the roof of the batholith between elevations 1400 and 1500 meters, between 1650 to 1700 metres depth, and at 2170 meters. Illite and quartz appear to be associated with hydrothermal processes induced by circulation in fault zones, precipitation is also described in the base interface although it is less than the precipitation of hematite. Chlorite and calcite show fairly similar behaviour with a regular distribution with depth although some areas of fractures are locally richer. This distribution may indicate a pervasive and relatively early process in the history of the massif, with an alteration of plagioclase feldspars, which allow the release of calcium to carbonate precipitation process.

Samples of different facies were selected and characterized from a petrophysical perspective. Particular attention was paid to the porosity and its location with regard to strain and alteration features and to the induced permeability and thermal conductivity.

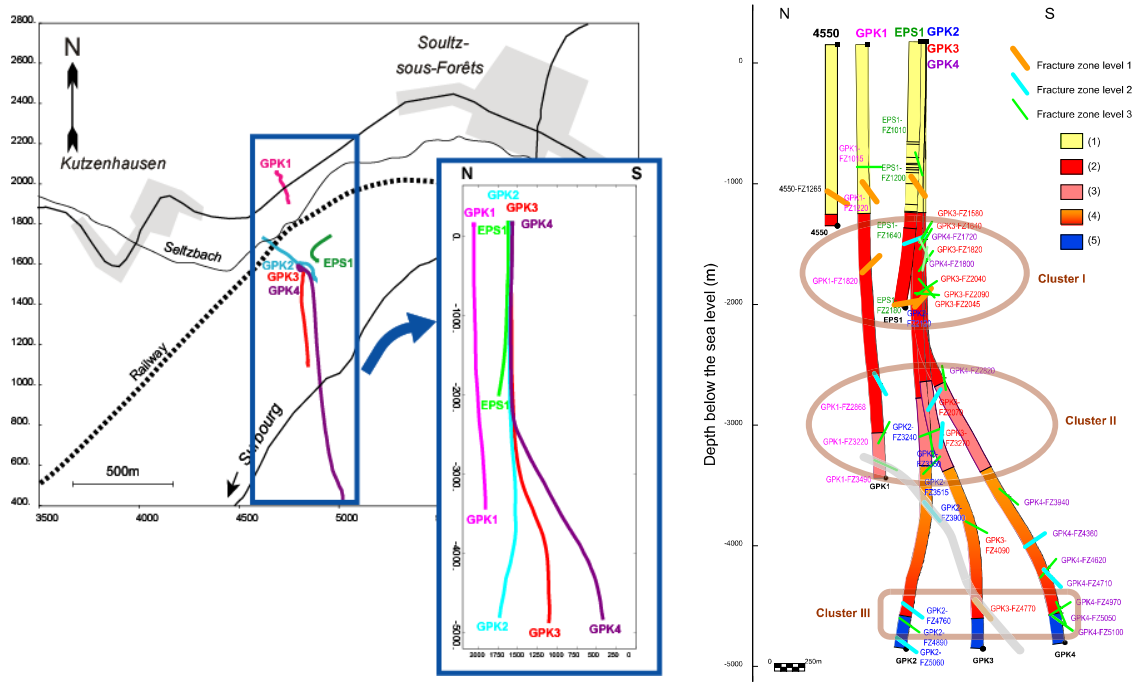

Figure 1: Right: Map view and vertical view of the set of boreholes. Left: Petrographic composition, fracture localisation and clusters of fractures described along the borehole (in Dezayes et al., 2010).

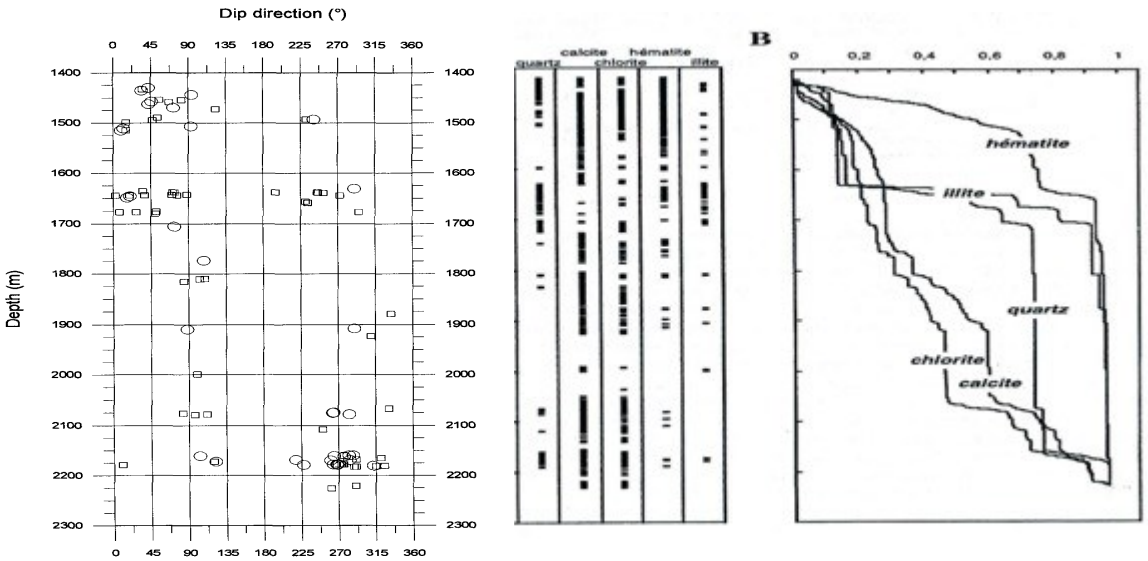

Figure 2: Dip direction of the fractures recognized along the borehole EPS1, and secondary minerals distribution (Sausse, 1998)

Facies	Primary mineralogical composition	Structure	alteration phases
Fresh	Porphyric granite with K-feldspars phenocryst, matrix is composed by quartz, plagioclases, biotite, K-feldspars	microcraking	
Hydrothermal alteration with chlorite (AHCS)		Microcraking, and light matrix alteration	Plagioclase and biotite partly changed in chlorite and sericite
Hydrothermal alteration with hematite (AHH)		Microcraking, medium matrix alteration	Plagioclase and biotite are changed by clays and carbonates, chlorite and illite, high content in hematite
hydrothermal alteration with illite (AHI)		Microcraking, fracturation, medium to high matrix alteration	Plagioclases and biotite are changed by clays and carbonates, chlorite and illite,
Hydrothermal alteration and cataclasis with hematite (AHCH)		Cataclasis with medium alteration index	Plagioclases and biotite are changed by clays and carbonates, chlorite and illite, high content in hematite
Hydrothermal alteration and cataclasis and silicification (AHCS)		Very high decrease of the grain size, the primary texture disappears	Large infilling of the fractures and matrix porosity by silicea.

Figure 3: Description of the secondary facies recognized along the borehole EPS1

3. PETROPHYSICAL TECHNIQUES

The first petrophysical parameter determined on these samples was the porosity. Porosity was measured using several techniques: mercury injection test, He picnometer, and water saturation. All the results were in agreement and only small differences were recorded within a five percent variation. Sample sizes varied from a few cm^3 to one dm^3.

Permeability was measured using a confining cell and a Nitrogen flux, performed under 10 bars of confining pressure and six and eight bars of head pressure. Flow measurements were carried out through mass flowmeters with appropriate ranges to determine permeability values between 10^{-19} m^2 and 10^{-12} m^2. The measurements were performed on cylindrical samples with diameter values between 14 and 25 mm and length values between 10 and 30 mm. At least four measurements were taken per sample for various pressure gradients.

For the determination of the thermal conductivity, the thermal conductivity scanner (TCS) process developed by Popov et al. (1999) was used. The TCS technique did not require any special sample preparation. It allowed the measurement of thermal conductivity values between 0.2 and 70 $W.m^{-1}.K^{-1}$ with an error equal to three percent of the measured value. The resolution of this device was about 1 mm^2, depending on the speed of movement of the block-source sensors. The results were in the form of a conductivity profile corresponding to all the measured points. The value of saturated porosity was calculated based on the measurements made on the same dry and saturated sample. This device was likewise used to construct maps of porosity by acquiring lines spaced one mm apart on dry and saturated samples.

4. PETROPHYSICAL PROPERTIES

4.1 Porosity

It is important to note that the reported porosity values are the connected porosity of the matrix consisting of the intragranular porosity induced by cracking of the grains or by alteration of certain mineral phases and intergranular or transgranular porosities from the fissure category. The fracture porosity is not included in this pore volume.

The measured porosity values vary between 0.1 and 15 percent, the higher values are measured for the level of 1650 metres, with a maximum porosity of 15 percent. At depths of up to 2175 metres, the maximum porosity is 13 percent. The altered upper zone has a maximum porosity of 10 percent (Figure 3). Areas of secondary fractures show intermediate values of matrix porosity with values less than five percent. In areas of high porosity, the porosity is not homogeneous. Some samples had very low porosities corresponding to fresh matrix volume. Thus, these deformation zones are marked by heterogeneous porosity values caused by the complex organization of the internal structure of these zones. This heterogeneity has two origins. First, the heterogeneity is related to the size of the samples used for the measurement. The impact of the sample size to heterogeneity is dependent on the mineralogical content of the sample. The mineralogical content is also significant to the heterogeneity of the porosity at granular scale. The four major mineral phases present in the material are: quartz, alkali feldspar, plagioclase, and micas. These minerals will not show the same volumes and pore structures. The feldspars present a matrix porosity associated with a replacement by illite or calcite. On the other hand, the micas have a porosity related to the precipitation of chlorite or smectite, while quartz represents crack porosity. The second source of heterogeneity is a real heterogeneous distribution of porosity in the rock above the decimetre

scale corresponding to a structural heterogeneity mainly controlled by the deformation scales. This point is illustrated by the porosity mapping obtained from thermal conductivity measurement process.

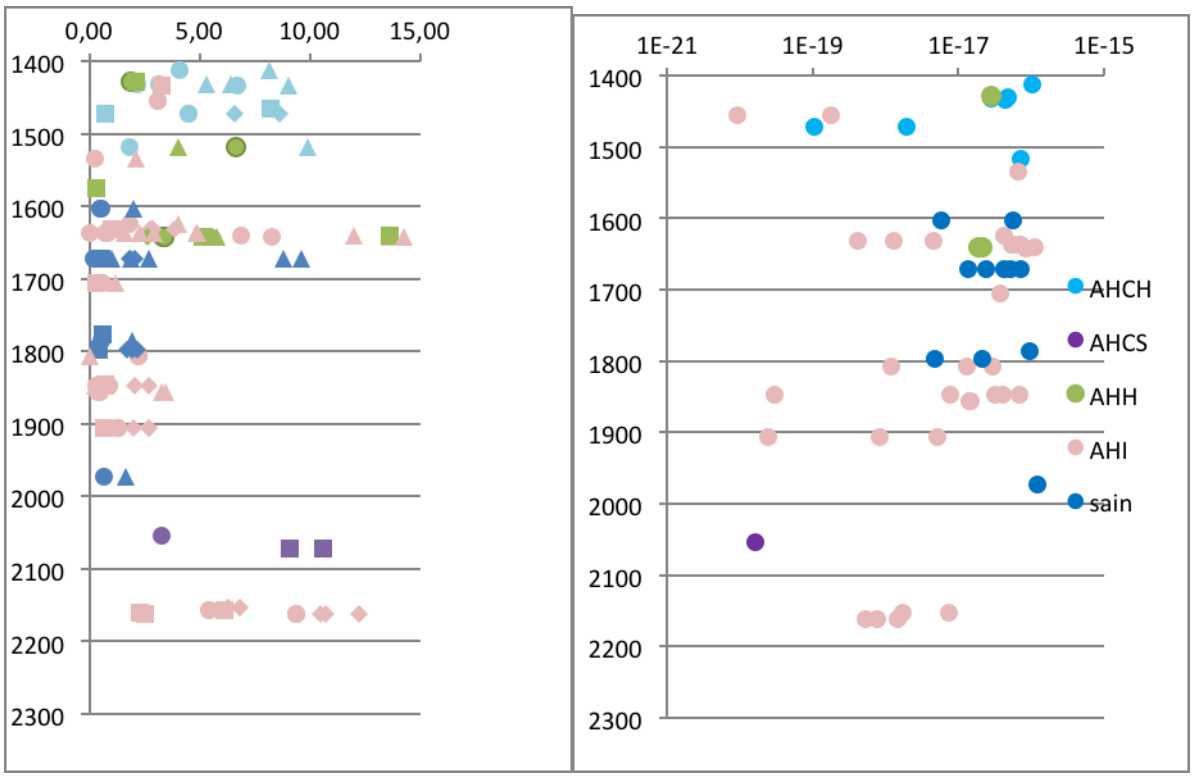

Figure 4: Distribution of the porosity value (right) and permability (left). Facies are describe in the table 1 (sain: fresh granite)

4.2 Permeability

The measured values vary over four orders of magnitude between 10^{-20} m^2 for the lowest and 10^{-16} m^2 for the highest values (Figure 4). Similar to porosity, the heterogeneity of permeability values have a two possible sources: sample heterogeneity and structural heterogeneity. However, the permeability is less discriminating in terms of deformation structures of secondary faults that are also permeable zones of major faults. This behaviour can be related to the structure of the porous network. Indeed, the elements of the network, including the shape and size of voids, will have a decisive role on the value of the transfer property. A first analysis of the porosity-permeability relationship was made by Rosener (2007) where it was showed that porosity-permeability relationships depended on the components of the porosity. For instance, it is possible to have samples with low permeability and high porosity. Samples that show the highest permeability values are those that have the lowest porosity (below two percent) but have crack-like structures (Surma, 2003 and Rosener, 2007). For the highest porosity regions, the permeability stabilizes at around 10^{-18} m^2 which corresponds to the strong development of matrix porosity in highly weathered samples and corresponding to matrix permeability.

4.3 Thermal conductivity

The average thermal conductivity values measured on dried samples are between 2 and 3.5 $W.m^{-1}.K^{-1}$ with rare values above 4 $W.m^{-1}.K^{-1}$ values (Figure 4). These high values are due to the presence of quartz vein zones or quartz cementation. The thermal conductivity values appear to be unrelated with petrographic or specific alteration facies. The lowest values are found in samples that have little or no quartz and for samples that contain quartz but are also porous in order to compensate for the increase in thermal conductivity caused by the presence of quartz. This lack of correlation is due to the relationship between the density and the size of the samples. Samples that are too small compared to the volume representation of the elementary material may have a significant mineralogical heterogeneity that can induce a significant variation in the measured value due to the high contrast in the thermal conductivity of different mineral phases.

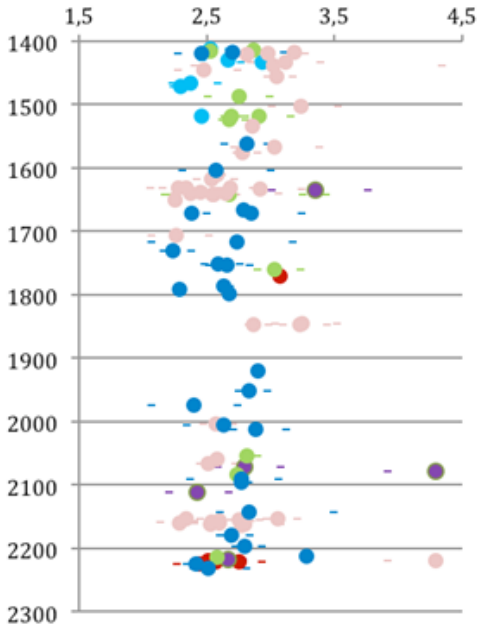

Figure 5: Thermal conductivity distribution vs depth.

5. THE MESOSCALE MAPPING OF THE POROSITY USING THERMAL CONDUCTIVITY MAPS

For the distribution of the porosity from the millimetre to centimetre scale, a protocol using optical scanning for thermal conductivity measurement (Popov et al., 1999) was developed. This method was done by comparing two thermal conductivity maps. The first map was carried out on the dry sample while the second map was made on the same sample saturated with water. The thermal conductivities of the air and water are respectively 0.59 and 0.0257 $W.m^{-1}.K^{-1}$, and the conductivity contrast allowed the location of the connected porosity between the dry state and saturated condition. Using a set of samples with characteristics petrographic composition and structures, the location of the porous network was determined.

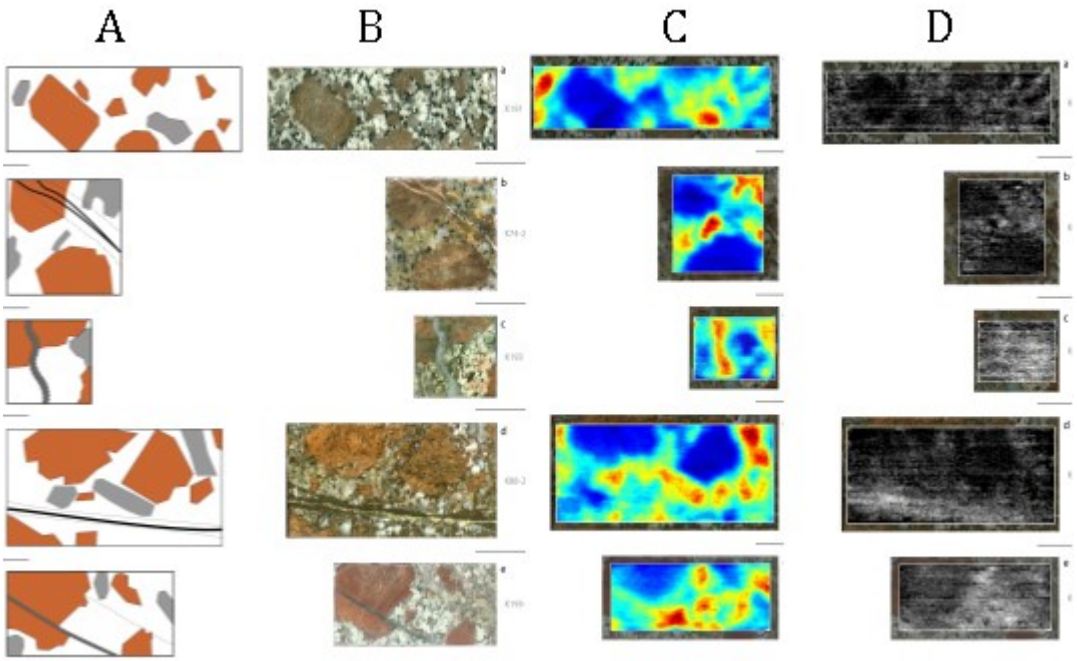

Figure 6: Column A: Schematic representation of the samples: brown : K-feldspars, grey, high quartz content, black line, fractures. Column B: view of the samples, from the top to the bottom, fresh granite (K191), chlorite and sericite alteration (K74), illite alteration (K193), fracture within a sample with hematite (K88), fracture within a sample with illite (K195). Column C: Thermal conductivity image for dry sample, column D, porosity maps (from Rosener, 2007)

Several common features were identified (Figure 6). Phenocrysts of feldspar had the lowest thermal conductivity and were areas with zero porosity. In general, the thermal conductivity variations were induced by local variations in mineralogy, and in particular by the presence of quartz, which corresponded to the high values of conductivity. On the other hand, areas of low conductivity corresponded to either areas where plagioclase feldspars were abundant or areas of high porosity. Some specific areas were also identified on the card including the thermal conductivity and the presence of cracks in the quartz for K191 and K195. The presence of hematite in feldspars sample K88, did not lead to increased local thermal conductivity. The organization of the porosity was

different depending on the state of alteration and structure. For fresh material, the porosity was distributed throughout the matrix, although the value of the porosity was low. The presence of fracture led to the development of porosity to the walls of these fractures and faults, regardless of the nature of the filling. The extension of this porosity from the footwall was used to characterize the damaged area that developed around these discontinuities. The thickness of the damaged area was multi-centimetres for fractures that had aperture values in millimetres. A second type of porous zone developed in the matrix of altered samples and especially in potassium feldspars or plagioclase. The two types of porous zones, fractures and altered matrix, were connected and the matrix alteration zones appeared to develop from areas of cracking.

6. THE POROSITY/PERMEABILITY RELATIONSHIP

The measured permeability values were between 10^{-14} m^2 and 10^{-20} m^2 for less than 12 percent porosity (Figure 7). The relationship within the three groups (Rosener and Géraud, 2007) was found by redefining the groups based on the structures that have dependent porosity. A larger number of samples was used to redefine the distribution with a larger number of groups. Group A, having a porosity of less than two percent and very low permeability, was comprised of slightly altered samples. In contrast, the samples of group B had low porosity (less than two percent) and permeability values that varied to over four orders of magnitude. The porous structure in group B was composed mainly of cracks and these samples showed the greatest variability in permeability. Permeability was directly related to the density of cracks and the interconnectivity of these structures. Group C samples had porosity values between two and five percent which corresponded to the variation between the natural porosity and the crack porosity in the pore matrix induced by alteration. These samples had a variable permeability depending on the proportion of cracks in the porous network and relatively small breakdown induced by the alteration. Samples in group D had higher porosity and permeability values in the order of 10^{-18} m^2. Group D samples showed a matrix porosity related to the alteration of primary phases which seems to be true for samples with porosity greater than five percent. This observation suggested that the porosity as a matrix array sufficiently developed to allow the transfer of fluid in the same matrix material. The structural integrity of these materials did not allow for the development of a network of cracks effective for transporting fluids.

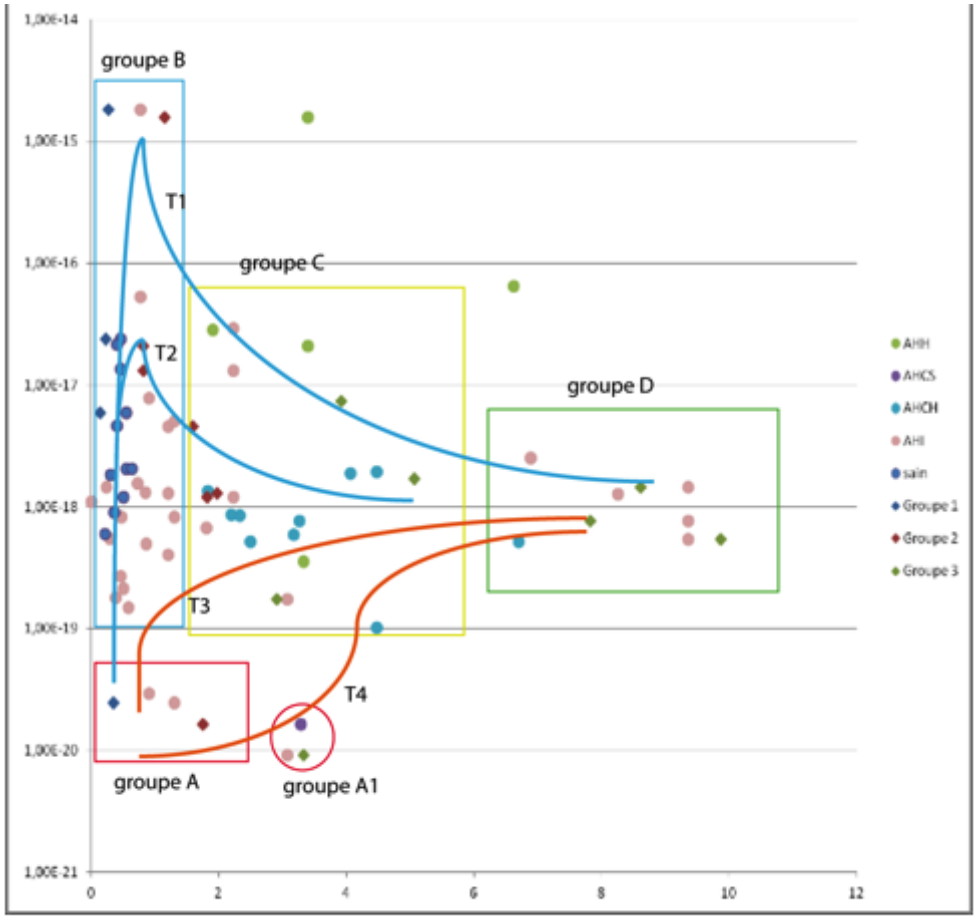

Figure 7: Distribution of groups of samples with reference to their structures, and different pathways to the porosity-permeability relationship behaviour.

7. THE POROSITY/PERMEABILITY BEHAVIOR IN SPACE AND TIME

The general pattern of porosity development related to alteration and mineralogical transformations proposed by Nishimoto (2010) corresponds to the penetration of hydrothermal fluids in the matrix through the network of cracks initially implemented in the damaged area of the fracture or fault. The interaction between the fluid and the rock is in a timeline that can be represented by a side profile with respect to the fracture. The early stages of the alteration are described in farther fractures while later stages are described with fractures near phyllitiques facies. In the outer zone, the fluids induce the dissolution of silica, potassium, calcium

feldspar, and mica. These elements are drained through the cracks which increases the sizes of structures to fracture zones . In the intermediate area of the fracture, Fe phyllosilicates are mobilized and can precipitate in the form of oxides and hydroxides in feldspars and micas, silica, calcium and potassium. Fe phyllosilicates continue to migrate into the network of pores and cracks where illite grains precipitated. In close fractures or isolated fractures, illite, quartz, and carbonates that are rich in iron will precipitate. In this schema, alteration must be added by supergene weathering processes concerning the outermost part of the batholith. This alteration is associated with the destabilization of iron oxides, magnetite, hematite, and is marked by a drop in signal magnetic susceptibility (Just and Kontny, 2012) .

A model of the spatial organization of porosity can be provided by using a segmentation-dependent alteration of the fault zone or fracture (Figure 7). Near large cracks or fissures of the most mature regions, a strong development of the alteration and porosity of pores in the area phyllitic facies will be observed. Moving away of the main cracks, porosity decreases with alteration. A switchover of fresh material may mark a zone where the porosity may be composed by crack. Due to the development of this crack porosity, a high permeability zone can develop between the weathered zone and the fresh zone. The organization of the groups of porosity and permeability can provide a change in time of the relationship. Two main types of evolution or development mechanism of porosity and permeability can be observed. The group A samples represent materials with little or no deformation. Group A involves a damaged area around the fracture and the corresponding paths in the T1 and T2 areas. The damaged area results from the development of a crack porosity (group B) which leads to a strong increase in permeability. Fluid flow is facilitated which allows the development of alteration and porosity. The increased tortuosity of the network, mainly because of the development of clays, lead to a drop in permeability and stabilization around a value of 10^{-18} m^2 (groups C and D). The difference between the paths of T1 and T2 is due to development of cracks and the porosity. The second type of path corresponds to the case where the development of the damaged area, consisting of cracks around the fracture, is small. In this case, the development of the porous zone is by propagation through the network of alterable mineral phases (mainly feldspars) which may form a continuous network in the matrix material. There is a gradual increase in permeability from 10^{-20} to 10^{-18} m^2 without going through maxima around 10^{-16} m^2. Two cases can be considered. The first is where the alteration results in the formation of the network of an effective network for transport path T3. An initial phase of increased permeability is induced by a small change in porosity (passage of group A at the base group B or group C and group D). The second case, T4, is where the connectivity of alterable phases does not allow the development of an effective network for transport. The porosity value must be in the order of 4 % for a permeable network to achieve the value of 10^{-18} m^2. This path corresponds to the sequential evolution with groups A, A1, C, and D.

On a larger scale, typically hectometre to kilometre in size, the organization of porosity in a granite massif will depend on the organization of the network of faults and fractures (Place et al., 2010) (Figure 8). The porosity, regardless of the type of structures that compose it, will be greater in the damaged area compared to the rest of the solid area. This damaged area also has increased permeability relative to the matrix. The permeability contrast will be three to five orders of magnitude depending on the type of structures that make up the porous network. The most important insights are achieved for crack networks with little or no alteration and precipitation of clay.

REFERENCES

Bartier, D., Ledésert, B., Clauer, N., Meunier, A., Liewig, N., Morvan, G. and Addad, A., 2008. Hydrothermal alteration of the Soultz-sous-Forêts granite (hot fractured rock geothermal exchanger) into a tosudite and illite assemblage. European Journal of Mineralogy, 20: 131-142.

Dezayes, C., Genter, A. and Valley, B., 2010. Structure of the low permeable naturally fractured geothermal reservoir at Soultz. C.R. geoscience, 342: 517-530.

Genter, A. and Traineau, H., 1992. Borehole EPS1, Alsace, France. Preliminary geological results from granite core analysis for hot dry rock research. Scientific drilling(3): 205-214.

Géraud, Y., Rosener, M., Surma, F., Place, J., le Garzic, E. and Diraison, M., 2010. Physical properties of fault zones within a granitic body : example of the Soutz-sous-Forêts geothermal site. C.R. geoscience, 342: 566-574.

Just, J. and Kontny, A., 2012. Thermally induced alterations of minerals during measurements of the temperature dependence of magnetic susceptibility : a case study from the hydrothermally altered Soultz-sous-Forêts granite, France. International Journal of Earth Sciences, 101: 819-839.

Ledésert, B., Hebert, R., Genter, A., Bartier, D. and Clauer, N., 2010. Fractures, hydrothermal alterations and permeability in the Soultz Enhanced Geothermal System. C. R. Geoscience, 342: 607-615.

Nishimoto, S. and Yoshida, H., 2010. Hydrothermal alteration of deep fractured granite: effects of dissolution and precipitation. Lithos, 115: 153-162.

Place, J., Sausse, J., Diraison, M., Géraud, Y. and Naville, C., 2011. 3D mapping of permeable structures affecting a deep granite basement from isotropic 3C VSP data. Geophysical Journal International: doi: 10.1111/j.1365-246X.2011.05012.x.

Popov, Y.A., Pribnow, D.F.C., Sass, J.H., Williams, C.F. and Burkhardt, H., 1999. Characterization of rock thermal conductivity by high-resolution optical scanning. geothermics, 28: 253-276.

Rosener, M. and Géraud, Y., 2007. Using physical properties to understand the porosity network geometry evolution on gradually altered granites in damage zones. , Rock Physics and Geomechanics in the Study of Reservoirs and Repositories. Special Publication of Geological Society of London, london, pp. 175-184.

Sausse, J., 1998. Caractérisation et modélisation des écoulements fluides en milieu fisuré. Relation avec les altérations hyrothermales et quantification des paléocontraintes., université Nancy 1, 336 pp.

Surma, F., 2003. Relation entre les caractéristiques minéralogiques, chimiques et physiques des matériaux granitiques du site géothermique de Soultz-sous-Forêts. PhD Thesis, Université Louis Pasteur, strasbourg, 321 pp.

Younes, A.I., Engelder, T. and Bosworth, W., 1998. Fracture distribution in faulted basement blocks : Gulf of Suez, Egypt. In: M.P. Coward, T.S. Daltaban and H. Johnson (Editors), Structural geology in reservoir characterization. geological society, special publications, london, pp. 167-190.